JCTC Journal of Chemical Theory and Computation

Article

pubs.acs.org/JCTC

Dynamic Multiscale Quantum Mechanics/Electromagnetics Simulation Method

Lingyi Meng,[†] ChiYung Yam,*[,†] SiuKong Koo,[†] Quan Chen,[‡] Ngai Wong,[‡] and GuanHua Chen*[,†]

[†]Department of Chemistry, The University of Hong Kong, Pokfulam Road, Hong Kong

[‡]Department of Electrical and Electronic Engineering, The University of Hong Kong, Pokfulam Road, Hong Kong

ABSTRACT: A newly developed hybrid quantum mechanics and electromagnetics (QM/EM) method [Yam et al. *Phys. Chem. Chem. Phys.* **2011**, *13*, 14365] is generalized to simulate the real time dynamics. Instead of the electric and magnetic fields, the scalar and vector potentials are used to integrate Maxwell's equations in the time domain. The TDDFT-NEGF-EOM method [Zheng et al. *Phys. Rev. B* **2007**, *75*, 195127] is employed to simulate the electronic dynamics in the quantum mechanical region. By allowing the penetration of a classical electromagnetic wave into the quantum mechanical region, the electromagnetic wave for the entire simulating region can be determined consistently by solving Maxwell's equations. The transient potential distributions and current density at the interface between quantum mechanical and classical regions are employed as the boundary conditions for the quantum mechanical and electromagnetic simulations, respectively. Charge distribution, current density, and potentials at different temporal steps and spatial scales are integrated seamlessly within a unified computational framework.

INTRODUCTION

The interaction between charge and electromagnetic field plays an essential role in many novel devices and materials such as transistors,[1−4] photovoltaic devices,[5] and metamaterials.[6,7] Quantum mechanical calculations have been carried out to study these devices and materials. Nonetheless, the calculations are often limited to small portions of these systems due to the computational costs. To simulate the entire system, Maxwell's equations coupled with the drift-diffusion equation for charge transport are often employed and solved.[8] This approach suffers from the neglect of quantum effects and atomistic details. To circumvent the deficiencies of both approaches, we have developed a hybrid method which combines quantum mechanics (QM) and electromagnetics (EM), the QM/EM method.[1]

The region where quantum effects and atomistic details are important is modeled with quantum mechanics, and the rest of the system is modeled with Maxwell's equations and the drift-diffusion equation.[1] The QM/EM method was developed for static fields. Time-dependent phenomena or processes are nevertheless important, for instance, the photoinduced charge separation and transport in photovoltaic devices,[9−11] transient current in transistors,[2,3] and dynamic dielectric response of metamaterials.[6,7] In this work, we extend the QM/EM method to the time domain which allows for the description of dynamic properties. In the time-domain QM/EM method, the electronic dynamics within the QM region are modeled by time-dependent density-functional theory[12] (TDDFT), and Maxwell's equations are employed to simulate the electromagnetic response.

As a rigorous extension of density-functional theory (DFT), TDDFT[12] is well suited for investigating real-time dynamics of many-electron systems in the QM region. In recent years, TDDFT has been used to simulate nanoelectronic devices, and there exist linear-scaling techniques to improve the efficiency.[13,14] Several TDDFT-based methods have been proposed[15−22] to model the time-dependent currents through molecular and nanoscopic devices. On the basis of the time-dependent holographic theorem, we have established a TDDFT formulation for open systems,[16,23] which combines TDDFT with the nonequilibrium Green's function (NEGF)[24] technique under adiabatic wide band limit (AWBL) approximation. The equation of motion (EOM) of the reduced single-electron density matrix for the device region is propagated in real time. This TDDFT-NEGF-EOM method[16,23] had been successfully applied in our earlier work.[2,3] The formalism can be readily extended to model the interactions between charge and light and thus be applied to study photoinduced transport, optoelectronic devices, metamaterials, and etc.

Maxwell's equations have been used to model a wide range of EM phenomena and devices such as antenna, photonic devices, metamaterials, and integrated circuits.[25,26] Charge transport has been modeled by the drift-diffusion equation.[8] The coupled EM and classical-charge-dynamics approaches have been developed and applied to model electronic devices, interconnects, substrates, and dielectrics.[27−31] A more sophisticated frequency-domain technique for multidomain (metal, semiconductor, and insulator) coupled simulation was proposed previously,[32,33] based on the finite volume method (FVM)[34] that guarantees charge conservation. Instead of the electric field $\bar{E}$ and the magnetic field $\bar{H}$, device properties are described by a scalar potential V and a vector potential $\bar{A}$ (with $\bar{B} = \nabla \times \bar{A}$).[25] The electron and hole densities are taken as independent variables for semiconductor materials. As a consequence, this technique provides a convenient and physically consistent approach to combine the full EM model and the Technology Computer Aided Design (TCAD) device model. Its solver has been transferred into a series of commercial tools of MAGWEL.[35] For the frequency-domain solution, corresponding equations are obtained

Received: November 29, 2011
Published: February 29, 2012

by Fourier transformation of the electromagnetic equations in the time domain.[26] Therefore, one can achieve the simplicity of the frequency-domain solver by assuming the system being excited by a sinusoidal perturbation with small amplitude (the small-signal assumption), which results in a pure time-harmonic solution.[26] Obviously, these assumptions limit the application of frequency-domain solution, especially as most external excitation signals do not satisfy the small-signal assumption and sometimes one could argue the validity of the method to describe the "switch-on" effect. On the other hand, in many existing time-domain EM methods, the carrier dynamics do not couple with the full wave dynamics.[36,37] All of these motivate the development of the coupled time-domain EM and classical charge carrier dynamics method with potentials V and $\bar{A}$ and charge densities as fundamental variables. This time-domain EM-TCAD solver can be used in conjunction with QM methods.[16,23] The potential V at the interface between the QM and EM regions calculated by the EM solver may be used as the boundary condition for the QM method. In return, the current density at the interface resulting from the QM calculation can be used as a part of the boundary condition for the EM solver.

In our previous work,[1] the QM/EM method has been tested against a full QM calculation in the static field regime. This has validated our overall QM/EM approach and the treatment of interfaces. In this work, we extend the static QM/EM method to the real time-domain for dynamic properties.

MODELS AND METHODS

In the time-domain QM/EM method, the whole device system is partitioned into the classical EM region and the QM region. To realize the seamless coupling between the EM and QM simulations, the electromagnetic wave dynamics for the entire system are solved by using Maxwell's equations. In the meantime, the current density and charge distribution in the QM region are calculated quantum mechanically. The drift-diffusion equations for the EM region link the current density to the electric field and the free carrier densities. The current-continuity equation is thus satisfied everywhere.

1. Electromagnetics Simulation. *I. Maxwell's Equations.* The electromagnetic characteristics inside and outside a given device can be determined by solving Maxwell's equations. EM solvers employ Maxwell's equations to describe the temporal and spatial evolution of the EM fields.[25,38] The differential forms for Maxwell's equations are as follows:

Gauss's law for electricity:

$$\nabla\cdot\bar{D} = \rho \tag{1}$$

Gauss's law for magnetism:

$$\nabla\cdot\bar{B} = 0 \tag{2}$$

Maxwell–Faraday's law:

$$\nabla \times \bar{E} = -\frac{\partial}{\partial t}\bar{B} \tag{3}$$

Maxwell–Ampere's law:

$$\nabla \times \bar{H} = \bar{J} + \frac{\partial}{\partial t}\bar{D} \tag{4}$$

where $\bar{D}$, $\bar{E}$, $\bar{B}$, and $\bar{H}$ denote the electrical induction, the electric field, the magnetic induction, and the magnetic field, respectively. And ρ and $\bar{J}$ denote the charge and current densities, respectively.

A. Constitutive Equations. The following constitutive relations are employed to relate $\bar{D}$ and $\bar{B}$ to $\bar{E}$ and $\bar{H}$:

$$\bar{D} = \varepsilon\bar{E} \tag{5}$$

$$\bar{B} = \mu\bar{H} \tag{6}$$

where ε and μ are the material permittivity and permeability, respectively. In the following simulations, we assume the permittivity ε is real, and the structure is nonmagnetic, i.e., $\mu = \mu_0$.[32,33]

B. Potential Description. In the theory of electromagnetic radiation, the original Maxwell's equations using vector fields $\bar{E}$ and $\bar{H}$ as basic variables can be rewritten as an alternative version based on the (electric) scalar potential V and (magnetic) vector potential $\bar{A}$, exploiting the transform relations[25]

$$\bar{B} = \nabla \times \bar{A} \tag{7}$$

$$\bar{E} = -\nabla V - \frac{\partial}{\partial t}\bar{A} \tag{8}$$

which are derived from Gauss' law for magnetism and Maxwell–Faraday's law.

Combined with eqs 7 and 8, eqs 1 and 4 are rewritten as

$$\nabla\cdot\left[\varepsilon\left(-\nabla V - \frac{\partial}{\partial t}\bar{A}\right)\right] - \rho = 0 \tag{9}$$

$$\nabla \times \left[\frac{1}{\mu}(\nabla \times \bar{A})\right] - \left[\bar{J} + \frac{\partial}{\partial t}\left(\varepsilon\left(-\nabla V - \frac{\partial}{\partial t}\bar{A}\right)\right)\right] = 0 \tag{10}$$

The reason for using potential description is two-fold. First, in potential formulation, a vector problem (electric field $\bar{E}$) is reduced to a scalar one (scalar potential V).[25] Second, these potential solutions are directly related to commonly used physical quantities in experiments, for instance, bias voltage.

C. Gauge Condition. It is an apparent advantage that only four components of variables need to be determined in eqs 7–10, in contrast to the six components in the vector field description in eqs 1–4. However, as a trade-off, potentials $\bar{A}$ and V are not uniquely determined by any given $\bar{E}$ and $\bar{B}$, i.e., the gauge freedom. An additional constraint, gauge condition, is required to cope with such a degree of freedom. Two commonly used gauge conditions are Coulomb gauge and Lorentz gauge.[25] Without a loss of generality, Lorentz gauge is employed throughout the numerical simulations as

$$\nabla\cdot\bar{A} + \mu\varepsilon\frac{\partial}{\partial t}V = 0 \tag{11}$$

D. Time Derivative of Vector Potential. To avoid the evaluation of the second-order time derivative of $\bar{A}$ in eq 10, a new variable $\bar{\Pi}$, which is the first-order time derivative of $\bar{A}$, is introduced:

$$\bar{\Pi} = \frac{\partial}{\partial t}\bar{A} \tag{12}$$

By introducing this new variable, Maxwell's eqs 9 and 10 are rewritten as

$$\nabla\cdot[\varepsilon(-\nabla V - \bar{\Pi})] - \rho = 0 \tag{13}$$

$$\nabla \times \left[\frac{1}{\mu}(\nabla \times \bar{A})\right] - \left[\bar{J} + \frac{\partial}{\partial t}(\varepsilon(-\nabla V - \bar{\Pi}))\right] = 0 \tag{14}$$

At this stage, only first-order time derivative terms are involved in eqs 13 and 14, which can be readily solved using existing numerical algorithms.[39,40]

II. Current and Charge Densities. The constitutive equation that relates the current $\bar{J}$ to the electric field and the free carrier densities is determined by the medium being considered in the EM region.

For the conductors in the system, the current $\bar{J}$ is given by classical Ohm's law:

$$\bar{J} = \sigma \bar{E} \tag{15}$$

where σ is the conductivity of the conductor. The current density satisfies the current continuity equation, and no free charge densities need to be solved inside the conductor.

$$\nabla \cdot \bar{J} + \frac{\partial}{\partial t}\rho = 0 \tag{16}$$

In the dielectric, there are also no free charges, and the dielectric losses are neglected. Therefore, no current equation needs to be solved in insulators, and the corresponding dielectric constants remain real.[32,33]

For the semiconductors, the current due to electrons (or holes) is split into drift and diffusion terms:[8]

$$\begin{aligned} \bar{J}_n &= q\mu_n n\bar{E} + k_B T\mu_n \nabla n \\ &= q\mu_n n(-\nabla V - \bar{\Pi}) + k_B T\mu_n \nabla n \end{aligned} \tag{17a}$$

$$\begin{aligned} \bar{J}_p &= q\mu_p p\bar{E} - k_B T\mu_p \nabla p \\ &= q\mu_p p(-\nabla V - \bar{\Pi}) - k_B T\mu_p \nabla p \end{aligned} \tag{17b}$$

where n and p correspond to the electron and hole density, respectively. $\mu_{n(p)}$ is the mobility of the electron(hole). k_B denotes the Boltzmann constant and T, the temperature. The continuity equations for the electrons and holes are[8]

$$\nabla \cdot \bar{J}_n - q\frac{\partial}{\partial t}n - qR(n, p) = 0 \tag{18a}$$

$$\nabla \cdot \bar{J}_p + q\frac{\partial}{\partial t}p + qR(n, p) = 0 \tag{18b}$$

where R is the charge carrier generation rate. Finally, the total charge density is given as

$$\rho = q(p - n + N_D - N_A) \tag{19}$$

where N_D and N_A are the donor and acceptor concentrations due to the doping, respectively. Note that the dopant concentrations are assumed to be time-independent during the time evolution.

III. Spatial-Domain Discretization of System. A. Discretization Scheme. We apply a regular Cartesian grid in the following simulations. After discretizing the system into grids, all independent scalar and vector variables (including potentials and charge densities) are allocated at every node or link, as shown in Figure 1. To illustrate, a scalar potential V_i and charge densities n_i and p_i are associated to a node i in the computational grid; to a link between the node i and j, a vector potential A_{ij} ($A_{ij} = \bar{n}_{ij} \cdot \bar{A}$, where $\bar{n}_{ij}$ is the unit vector of the link) and its first time derivative Π_{ij} ($\Pi_{ij} = (\partial/\partial t)A_{ij}$) are associated. Those original vector variables ($\bar{A}$ and $\bar{\Pi}$) have been replaced by their scalar projections along a particular

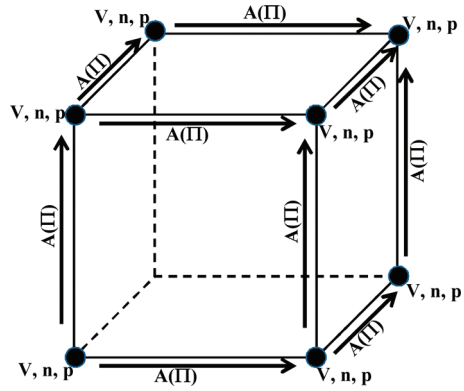

Figure 1. Fundamental variables allocated on a regular Cartesian cube.

link in the discretization scheme and eventually depend only on time after discretization.

To obtain physically correct results for high-frequency computations of electromagnetic problems, differential operators acting on variables need to take into account their geometrical origin.[32−34]

The gradient operator acting on the scalar potential can be discretized straightforwardly, and integrations over a perpendicular surface and along a link are given by eqs 20 and 21, respectively:

$$\int_{\Delta S_{ij}} \nabla V \, d\bar{S} = \frac{V_j - V_i}{h_{ij}} S_{ij} \tag{20}$$

$$\int_{\Delta L_{ij}} \nabla V \, d\bar{L} = V_j - V_i \tag{21}$$

where S_{ij} is the perpendicular surface of the link ij and h_{ij} is the link length. The divergence operator is discretized by converting the volume integration into its equivalent surface integration (the Gauss's theorem) as

$$\int_{\Delta V_i} \nabla \cdot (\varepsilon \nabla V) \, dv = \int_{\partial(\Delta V_i)} \varepsilon \nabla V \, d\bar{S} = \sum_{j=1}^{6} \varepsilon_{ij} S_{ij} \frac{V_j - V_i}{h_{ij}} \tag{22}$$

where the summation is over the six surfaces enclosing the volume.

Similarly, the divergence operator on the vector potential is discretized as

$$\begin{aligned} \int_{\Delta V_i} \nabla \cdot \bar{A} \, dv &= \int_{\partial(\Delta V_i)} \bar{A} \, d\bar{S} = \sum_{j=1}^{6} s_{ij} A_{ij} S_{ij}, \; s_{ij} \\ &= \text{sign}(n_j - n_i) \end{aligned} \tag{23}$$

where signs s_{ij} indicate the flux direction.

According to Stoke's theorem, the surface integration can be replaced by the line integration over the four links circling the surface. Therefore, the curl operator is discretized as

$$\int_{S_{ij}} \nabla \times \bar{A} \, d\bar{S} = \int_{\partial(S_{ij})} \bar{A} \, d\bar{l} = \sum_{k}^{4} A_k^{(ij)} h_k \tag{24}$$

On the basis of the discretization of the curl operator, the curl−curl operator for a link can be also discretized by borrowing the field $\bar{B}$ as an auxiliary variable, and more detailed information is available in refs 32 and 33.

B. Scharfetter–Gummel Discretization of Semiconductor Current. Besides these electromagnetic equations, the drift-diffusion equation for the semiconductor also needs to be discretized. Following the Scharfetter–Gummel discretization method,[41] with the "de Mari" scaling scheme, eq 17 becomes

$$J_{nij} = -\frac{\mu_{nij}}{h_{ij}} B[-(V_j - V_i + \Pi_{ij}h_{ij})]n_i + \frac{\mu_{nij}}{h_{ij}} B[+(V_j - V_i + \Pi_{ij}h_{ij})]n_j \tag{25a}$$

$$J_{pij} = \frac{\mu_{pij}}{h_{ij}} B[+(V_j - V_i + \Pi_{ij}h_{ij})]p_i - \frac{\mu_{pij}}{h_{ij}} B[-(V_j - V_i + \Pi_{ij}h_{ij})]p_j \tag{25b}$$

where the Bernoulli function $B(x)$ is defined as

$$B(x) = \frac{x}{e^x - 1} \tag{26}$$

IV. Time-Domain Integration Scheme. A. Explicit Scheme. On the basis of eqs 11, 14 and (18), the time derivatives of variables $\bar{\Pi}$, V, n and p can be readily calculated, with the "de Mari" scaling scheme:

$$-K\varepsilon\frac{\partial}{\partial t}\bar{\Pi} = \nabla \times (\nabla \times \bar{A}) - K\bar{J} + K\varepsilon\frac{\partial}{\partial t}\nabla V \quad \text{(Ampere's equation)} \tag{27}$$

$$-K\varepsilon\frac{\partial}{\partial t}V = \nabla\cdot\bar{A} \quad \text{(Lorentz gauge)} \tag{28}$$

$$q\frac{\partial}{\partial t}n = \nabla\cdot\bar{J}_n - qR(n, p) \quad \text{(continuity equation)} \tag{29a}$$

$$-q\frac{\partial}{\partial t}p = \nabla\cdot\bar{J}_p + qR(n, p) \quad \text{(continuity equation)} \tag{29b}$$

In eqs 27 and 28, the dimensionless constant $K = (1/c^2)(\lambda/\tau)^2$, where c is the speed of light in a vacuum, and λ and τ denote the scaling parameters for lengths and time in the scaling scheme, respectively.[33] And the Gauss equation, eq 13, in this explicit scheme is considered as a constraint condition to check the validity of the time-domain trajectory.

By ignoring the relativistic effects, eqs 27–29 constitute a series of self-consistent ordinary differential equations (ODEs) for all nodes and links in the system and can be first discretized by FVM in the spatial-domain as mentioned. To obtain the time-domain EM response, the Runge–Kutta methods including implicit and explicit iterative methods are adopted to numerically solve these ODEs.[39]

For the initial-value problem,

$$\frac{dy}{dt} = f(t, y), y(0) = y_0 \tag{30}$$

The general form of the Runge–Kutta methods for estimating the information at the next step is

$$y_n = y_{n-1} + \Delta t_n \sum_{i=1}^{s} b_i k_i \tag{31}$$

$$k_i = f(t_{n-1} + \Delta t_n c_i, y_{n-1} + \Delta t_n \sum_{j=1}^{s} a_{ij}k_j) \tag{32}$$

These parameters are summarized via the *Butcher tableau*:[40]

$$\begin{array}{c|cccc} c_1 & a_{11} & a_{12} & \cdots & a_{1s} \\ c_2 & a_{21} & a_{22} & \cdots & a_{2s} \\ \vdots & \vdots & \vdots & \ddots & \vdots \\ c_s & a_{s1} & a_{s2} & \cdots & a_{ss} \\ \hline & b_1 & b_2 & \cdots & b_s \end{array} = \begin{array}{c|c} \mathbf{c} & A \\ \hline & b^T \end{array} \tag{33}$$

For the explicit fourth-order Runge–Kutta method, the corresponding *Butcher tableau* is as follows:

$$\begin{array}{c|cccc} 0 & 0 & 0 & 0 & 0 \\ 1/2 & 1/2 & 0 & 0 & 0 \\ 1/2 & 0 & 1/2 & 0 & 0 \\ 1 & 0 & 0 & 1 & 0 \\ \hline & 1/6 & 1/3 & 1/3 & 1/6 \end{array} \tag{34}$$

According to the Courant stability condition,[42] the time step Δt used in the explicit Runge–Kutta method must satisfy

$$u_{\max}\Delta t \le \left[\frac{1}{\Delta x^2} + \frac{1}{\Delta y^2} + \frac{1}{\Delta z^2}\right]^{-1/2} \tag{35}$$

where $u_{\max}$ is the maximum wave phase velocity within the model. In practice, time evolution integration using such a small time step is highly inefficient for large-scale problems. Therefore, it is necessary to avoid the constraint of the Courant stability condition by using an implicit Runge–Kutta method.[38,40]

B. Implicit Scheme. The scalar potential V is solved by the Gauss law in insulators and semiconductors. For metals, the Gauss law together with the current-continuity equation is solved to evaluate V. The complete set of equations for V then reads

$$\begin{cases} \nabla\bullet[\varepsilon(\nabla V + \bar{\Pi})] + \rho = 0 & \text{insulator or semiconductor} \\ \nabla\bullet\left[\left(\sigma + \frac{\partial}{\partial t}\varepsilon\right)(\nabla V + \bar{\Pi})\right] = 0 & \text{metal} \end{cases} \tag{36}$$

In the semiconductor region, the electron and hole concentrations, n and p, can be solved by the current-continuity equation given by eq 18, and the current in semiconductor is determined by the drift-diffusion equation which is discretized as eq 25.

Furthermore, the vector potential $\bar{A}$ should be solved by the Ampere equation, eq 27, which governs the magnetic system. Equation 27 is however not well-defined since the curl–curl operator is intrinsically singular when discretized by FVM; i.e., one row of the resultant matrix is not linearly independent.[32,33] A smarter treatment in the EM solver that is implemented in the MAGWEL's tools is to subtract eq 27 from the divergence of the gauge condition, eq 11, which yields

$$\nabla \times (\nabla \times \bar{A}) - \nabla(\nabla\cdot\bar{A}) + K\frac{\partial}{\partial t}\varepsilon(\nabla V + \bar{\Pi}) - K\nabla\left(\varepsilon\frac{\partial}{\partial t}V\right) - K\bar{J} = 0 \tag{37}$$

This regulation procedure leads to a Laplacian-like operator acting on the vector potential $\bar{A}$ and thus eliminates the singularity. Finally, eqs 18, 25, 36, and 37 form a set of coupled

equations for the entire system, and we can express these equations in a more compact form:

$$F(V, n, p, \bar{A}, \bar{\Pi}, V', n', p', \bar{\Pi}') = 0 \tag{38}$$

where $(V', n', p', \bar{\Pi}')$ indicates the time derivative of $(V, n, p, \bar{\Pi})$.

According to the first order implicit Runge–Kutta method,[39,40] denoted as "IRK1" hereafter, for which the *Butcher tableau* is simply

$$\begin{array}{c|c} 1 & 1 \\ \hline & 1 \end{array} \tag{39}$$

eq 38 can be approximately solved as

$$F\left(V_n, n_n, p_n, \bar{A}_n, \bar{\Pi}_n, \frac{V_n - V_{n-1}}{dt}, \frac{n_n - n_{n-1}}{dt}, \frac{p_n - p_{n-1}}{dt}, \frac{\bar{\Pi}_n - \bar{\Pi}_{n-1}}{dt}\right) = 0 \tag{40}$$

where $(V_n\ n_n, p_n, \bar{A}_n, \bar{\Pi}_n)$ represents variables of the present (nth) step and $(V_{n-1}, n_{n-1}, p_{n-1}, \bar{\Pi}_{n-1})$ represents the variables at the last $(n-1)$th) step, and dt is the time interval. Actually, all we need to do is to solve eq 40 for every time step, by assuming that the previous history of the evolution system is known. To solve the nonlinear eq 40 at every time step, the Newton–Raphson method is applied to iteratively refine the solution until convergence. Eventually, a dynamic trajectory for the system can be obtained by repeating this procedure step by step.

To improve the accuracy, a second order implicit Runge–Kutta method[40] is used in our simulations, denoted as "IRK2" hereafter, and the *Butcher tableau* is

$$\begin{array}{c|cc} 0 & 0 & 0 \\ 1 & \frac{1}{2} & \frac{1}{2} \\ \hline & \frac{1}{2} & \frac{1}{2} \end{array} \tag{41}$$

V. Boundary Condition and Interface Condition. The boundary condition for the EM solver is the condition applied on the boundary of the whole simulation domain, while the interface conditions refer to the boundary conditions applied on the interfaces between different material subdomains that comprise the whole system.

We divide the boundary of the simulation domain into two parts: contact regions and noncontact regions. The contacts allow currents to enter and leave the simulation domain, wherein the constant voltage condition is applied. The remaining part of surface, the noncontact boundary, is characterized by requiring that the outward-pointing normal component of $\bar{E}$ vanishes, i.e., $\bar{E}_n = 0$. The boundary values of carrier concentrations n and p are determined by solving the current-continuity equation, similar to ordinary semiconductor nodes, but associate with a reduced volume. For the magnetic field, a similar requirement of $\bar{B}_n = 0$ is applied to keep all magnetic fields inside the simulation domain. This forces a zero tangential component of $\bar{A}$ since $\bar{B} = \nabla \times \bar{A}$. The boundary condition for the vector potential is therefore $\bar{A}_t = 0$, which holds for both the contact and noncontact boundaries.

In general, an on-chip structure consists of three types of materials, i.e., metal, semiconductor, and insulator, categorized mostly according to their electric properties. In practice, there are four major types of interfaces, at which the interface condition for the three basic electric variables, V, n, and p, need to be specified. Generally speaking, the boundary condition is that the current density is continuous at the interface.

At the metal/semiconductor interface, the scalar potential V at the interface is a double-valued variable with V_{metal} at the metal side and V_{semi} at the semiconductor side. The difference between the two potentials, $dV = V_{metal} - V_{semi}$, is the so-called built-in potential describing the height of the potential barrier formed when the two materials are connected. With the charge neutrality condition $p - n + N_d = 0$, where $N_d = N_D^+ + N_A^-$ is the net doping concentration, the built-in potentials are determined for n-type semiconductors ($N_d > 0$) and p-type semiconductors ($N_d < 0$) by

$$dV = \mathrm{In}\left(-\frac{N_d}{2n_i}\left(1 + \sqrt{1 + \frac{4n_i^2}{N_d^2}}\right)\right) \tag{42}$$

$$dV = -\mathrm{In}\left(\frac{N_d}{2n_i}\left(1 + \sqrt{1 + \frac{4n_i^2}{N_d^2}}\right)\right) \tag{43}$$

where n_i (=1 × 10^{24}/m^3 in our simulations) is the intrinsic concentration. When there is no dopant in the semiconductor ($N_d = 0$), the potential should be continuous across the metal/semiconductor interface ($dV = 0$). For doped semiconductors, dV can be readily determined from the doping concentration. Thus, at the metal/semiconductor interfaces, there is only one unknown V (either V_{metal} or V_{semi}) that needs to be solved (charge densities can be postprocessed after V is solved).

Similar treatment is applied to the "triple" points where the three types of materials join together. The scalar potential is triple-valued, and the governing equation is the current-continuity equation. For computational convenience, we assume the potential value for the insulator side being the average of the metal and semiconductor sides. At the metal/insulator interface, the scalar potential has to be continuous across the interface, and the current balance must be satisfied.

For the nodes at the semiconductor/insulator interface, there are three unknowns to be determined, V, n, and p. The variables are solved in a similar way to that done in the device simulation for the bulk of semiconductors; i.e., the Gauss equation is solved in conjunction with the current-continuity equation, while the potential is continuous across the interfaces. And more detailed information is available in refs 32 and 33.

VI. Static Analysis and Initial Guess. The time-domain solution of the coupled simulation should start with solving the static system by setting all time-dependent terms as zero; therefore, the governing equations simply become

$$\begin{cases} \nabla\cdot[\varepsilon\nabla V^0] + \rho^0 = 0 & \text{insulator or semiconductor} \\ \nabla\cdot[\sigma\nabla V^0] = 0 & \text{metal} \end{cases} \tag{44}$$

$$\nabla\cdot\bar{J}_n^0 - qR(n^0, p^0) = 0 \tag{45a}$$

$$\nabla\cdot\bar{J}_p^0 + qR(n^0, p^0) = 0 \tag{45b}$$

supplemented by the Scharfetter–Gummel expression of static semiconductor current J^0

$$\bar{J}_n^0 = q\mu_n n^0(-\nabla V^0) + k_B T\mu_n \nabla n^0 \tag{46a}$$

$$\bar{J}_p^0 = q\mu_p p^0(-\nabla V^0) - k_B T\mu_p \nabla p^0 \tag{46b}$$

The static component of $\bar{A}$ is then determined from the static current in a postprocessing step. The static solution (V^0, n^0, p^0, A^0) is then employed as the initial state for the time-domain EM solver.

In current simulations, all EM programs are coded and implemented in MATLAB, and we assume that there is no charge generation or recombination, i.e., the net charge generation rate $R(n,p)$ in current continuity equations for semiconductor equals zero.

VII. Comparison with Finite-Difference Time-Domain Method. The finite-difference time-domain (FDTD) method is another popular technique for multiphysics simulation owing to its simplicity and efficiency. Recent efforts in coupling FDTD EM solver with particle-based semiconductor simulators have been reported.[29,43] Our method based on FVM, despite sharing many commonalities with FDTD, as both rely on finite difference approximation, differs from FDTD-based frameworks in the following respects. First, the use of potential variable in our EM formulation greatly facilitates the coupling with the QM simulation, where potentials are much more well-defined than fields in QM dynamics. Although with certain approximation a solution in fields can be used to provide the QM solver with potential boundary conditions, it is still more physically consistent and numerically convenient to formulate the two systems with the same set of variables and avoid variable conversions. Second, carrier dynamics is usually of primary interest in multiphysics simulation, and local conservation of carrier/flux becomes an important requirement for numerical schemes. Standard FDTD, which is typically employed in a charge-neutral structure, has to be enforced by explicit inclusion of the Gauss law and the current continuity equation.[43] Our EM method also solves these two equations explicitly, and the FVM discretization has a built-in guarantee of local conservation. Last, standard FDTD is an explicit scheme where no solution of the linear system is involved. However, the small length scale usually requires excessively small time steps because of the Courant stability limit. In our EM method, the implicit time integration scheme is adopted to alleviate this constraint. Similar choice can also be found in the FDTD-related framework.[29]

2. Quantum Mechanics Simulation. In order to simulate realistic systems, computational efficiency has to be further increased. For the QM calculation, we employ the TDDFT-NEGF-EOM method[16,23] with the AWBL approximation and the density-functional tight-binding (DFTB) for electronic dynamics.[44,45]

I. Liouville–von Neumann Equation for Open Systems. We consider an electronic device connecting to left and right electrodes and simulate the current through the central device region (D) which is driven by a time-dependent bias potential $V(t)$. We follow the equation of motion of the reduced single-electron density matrix of the device region, given as

$$i\dot{\sigma}_D(t) = [h_D(t), \sigma_D(t)] - i\sum_{\alpha=L,R} Q_\alpha(t) \tag{47}$$

where h_D and σ_D denote the Fock and density matrix of the device, respectively, and Q accounts for the influence of the electrodes or gates. Equation 47 is the single-electron density matrix based Liouville–von Neumann equation. Following the Keldysh NEGF formalism,[46] $Q(t)$ can be expressed as

$$Q_\alpha(t) = \int_{-\infty}^{\infty} d\tau[\Sigma_\alpha^r(t,\tau)\, G^<(\tau,t) + \Sigma_\alpha^<(t,\tau)\, G^a(\tau,t)] - \int_{-\infty}^{\infty} d\tau[G^<(t,\tau)\,\Sigma_\alpha^a(\tau,t) + G^r(t,\tau)\Sigma_\alpha^<(\tau,t)] \tag{48}$$

Here, G^r, G^a, and $G^<$ are the retarded, advanced, and lesser Green's functions of the device region, respectively, and Σ_α^r, Σ_α^a, and $\Sigma_\alpha^<$ denote the retarded, advanced, and lesser self-energies due to electrode α, respectively, expressed as

$$\Sigma_\alpha^{r,a,<}(t,t') = h_\alpha^\dagger(t)\, g_\alpha^{r,a,<}(t,t')\, h_\alpha(t') \tag{49}$$

where $g_\alpha^{r,a,<}$ represents the surface Green's functions of the semi-infinite electrode α. It is noted that eq 49 involves matrices with dimensions of the device region only. Solving eq 48 for $Q(t)$ is computational demanding due to the two-time quantities involved. We adopt the AWBL approximation[16] for $Q(t)$. Within the AWBL approximation, the retarded and advanced self-energies become local in time:

$$\Sigma_\alpha^{r,a}(t,t') = i\delta(t-t')\Lambda_\alpha \tag{50}$$

where Λ_α denotes the imaginary part of self-energies evaluated at the Fermi energy. The lesser self-energy reads

$$\Sigma_\alpha^<(t,t') = \frac{2i}{\pi}\Lambda_\alpha \exp\left(i\int_{t'}^{t} d\tau \Delta V^\alpha(\tau)\right) \int_{-\infty}^{\infty} d\varepsilon f^\alpha(\varepsilon)\, e^{i\varepsilon(t-\tau)} \tag{51}$$

with f being the Fermi distribution and ΔV^α the applied voltage. With eqs 50 and 51 above, the dissipation term $Q(t)$ can be simplified[16,23] as

$$Q_\alpha(t) = \{\Lambda_\alpha, \sigma_D\} + P_\alpha(t) + [P_\alpha(t)]^\dagger \tag{52}$$

The first term involves an anticommutator describing the level broadening. Invoking an adiabatic approximation, $P_\alpha(t)$ is given by

$$P_\alpha(t) = \frac{-2i}{\pi}\Lambda_\alpha U_\alpha(t)\int_{-\infty}^{\mu_0} d\varepsilon \frac{e^{i\varepsilon t}}{\varepsilon - H(0) - \Sigma^r} - \frac{2i}{\pi}\int_{-\infty}^{\mu_0} d\varepsilon[I - U_\alpha(t)\, e^{i\varepsilon t}] \times \frac{1}{\varepsilon - \Delta V_\alpha - H(t) - \Sigma^r} \tag{53}$$

and the history of the applied voltage is tracked with the propagator $U_\alpha(t)$

$$U_\alpha(t) = \exp\left(-i\int_0^t d\tau[H(\tau) + \Sigma^r - \Delta V_\alpha(\tau)]\right) \tag{54}$$

Equations47 and 52 provide a practical scheme to solve the density matrix in real time, and the time-dependent current $I(t)$ passing through contact α is given by

$$I_\alpha(t) = -Tr[Q_\alpha(t)] \tag{55}$$

II. Density-Functional Tight-Binding Method. The above formalism has recently been implemented in the framework of the DFTB method[47] which provides an efficient way to simulate dynamic processes in quantum transport. The DFTB

method[44,45] is an approximate DFT method based on a second-order expansion of the Kohn−Sham total energy with respect to charge density fluctuations. In the framework of the DFTB method, the Hamiltonian matrix is constructed as

$$h_{ij}(t) = h_{ij}^{0}[\rho_0(r)] + \delta h[\Delta q_\alpha(t)] \tag{56}$$

where $\rho_0(r)$ is the density of a reference system, taken as a superposition of neutral densities from all constituent atoms. h^0 represents the Hamiltonian matrix of the corresponding reference system and is precomputed and stored as a function of the interelement distance. Δq_α is the change of Mulliken charge with respect to the reference system. Expanding Δq_α on real space, the potential in the device region is obtained by solving the Poisson equation:

$$\delta\rho(r, t) = \sum_\alpha \frac{\Delta q_\alpha(t)\tau_\alpha^3}{8\pi} e^{-\tau_\alpha|\mathbf{r}-\mathbf{R}_\alpha|} \tag{57}$$

$$\nabla^2\delta V(r, t) = -4\pi\delta\rho(r, t) + \left(\nabla\cdot\frac{\partial\vec{A}}{\partial t}\right)_{EM} \tag{58}$$

with boundary conditions being determined by applied voltages. Compared with the treatment in previous simulations,[2,3,16] the second term on the rhs of eq 58 is an extra correction to recover a full electrodynamics description for entire system including the QM region. In the QM/EM method, this term can be classically determined by EM modeling. δh is then obtained by projecting the potential back to the atomic sites:

$$\delta h_{ij}(t) = \frac{1}{2}S_{ij}[\int dr\ \delta V(r, t)(e^{-\tau_\alpha|\mathbf{r}-\mathbf{R}_\alpha|} + e^{-\tau_\beta|\mathbf{r}-\mathbf{R}_\beta|})],\ i \in \alpha,\ j \in \beta \tag{59}$$

In principle, the vector potential should be included in our Hamiltonian:[48]

$$\hat{H} = \frac{1}{2}\sum_k (\vec{p}_k + \vec{A}_k)^2 + \hat{V} \tag{60}$$

However, in our present work, the size of our system, in particular the QM region, is small compared to the wavelength; the effect coming from the vector potential is negligible. In fact, we indeed include the vector potential semiclassically in our QM simulations through the second term on the rhs of eq 58.

It should be emphasized that the QM method presented here is restricted to scalar potentials as a limitation of our current scheme. Actually, the time-dependent current-density functional theory[22,48] has been proposed to model situations involving vector potentials, where a time-dependent magnetic field is introduced into the QM domain.

3. Information Exchange between QM/EM Solvers. Information exchange between different models is a key issue[43] in our multiscale QM/EM simulations, as shown in Figure 2. Initially, the scalar potential distribution can be calculated by the EM solver for the whole system including the QM region. The potential on the boundary of QM region is used as the boundary condition for the TDDFTB method. Then, the time-dependent current density calculated with the QM method is fed back to the EM solver as the boundary condition for next QM/EM cycle.

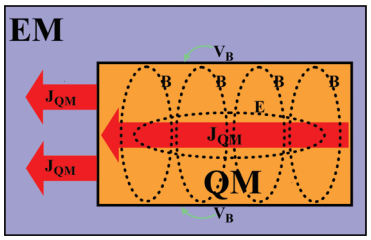

Figure 2. The information exchange between QM and EM methods. The classical electromagnetic wave could penetrate into QM region.

We solve Maxwell's equations in the QM region, instead of the Poisson equation. The corresponding equations for the time derivative of the scalar potential and vector potential in the QM region are given as follows:

$$\nabla\cdot\left[\bar{J}_{QM} + \frac{\partial}{\partial t}\varepsilon(\nabla V + \bar{\Pi})\right] = 0 \tag{61}$$

$$\nabla\times(\nabla\times\bar{A}) - \nabla(\nabla\cdot\bar{A}) + K\frac{\partial}{\partial t}\varepsilon(\nabla V + \bar{\Pi}) - K\nabla\left(\varepsilon\frac{\partial}{\partial t}V\right) - K\bar{J}_{QM} = 0 \tag{62}$$

where the conduction current density $\bar{J}_{QM}$ is calculated by the QM method. To be unified within the proposed EM framework, the QM region here is actually considered as a special "material", in which the constitutive equation relates the conduction current density to the electromagnetic field and the electron density is solely modeled quantum mechanically. Once the current density distribution from QM simulations is obtained, eqs 61 and 62 can be solved universally in the EM solver.

To precisely describe the electromagnetic environment in QM region, the built-in Poisson equation coupled with TDDFTB method is solved in the QM model to calculate the scalar potential and the conduction current. In addition, the corresponding time derivative of scalar potential and vector potential are determined by eqs 61 and 62 to estimate the displacement current across the QM region. As a result, Maxwell's equations have been approximately resumed for the QM region by these integration schemes, which lead to a reliable description for the electromagnetic environment in the QM region. The governing equations for the QM and EM regions have to be solved alternately to attain a global dynamics solution of the multiscale/multiphysics problems as shown in Figure 3.

In practice, grids in the QM domain are finer to capture the atomistic details while coarser grids are adopted in the EM domain. The potential from the EM solver must be interpolated to match the higher resolution of the QM solver. And conversely, the QM calculated current density at the interface should be integrated for the EM solver.

It should be noted that the application of our QM/EM method is not limited to materials with a real permittivity. Phenomena like plasmon behavior and absorption can be captured by including a complex permittivity in our QM/EM method. In such a case, we just need to add the complex conjugate of the potential energy to the Hamiltonian. For the QM part, whereas an approximate DFT, the DFTB method, is adopted, no physical parameter is used in the Hamiltonian. The response of the system to external fields can be thus considered as modeled from first

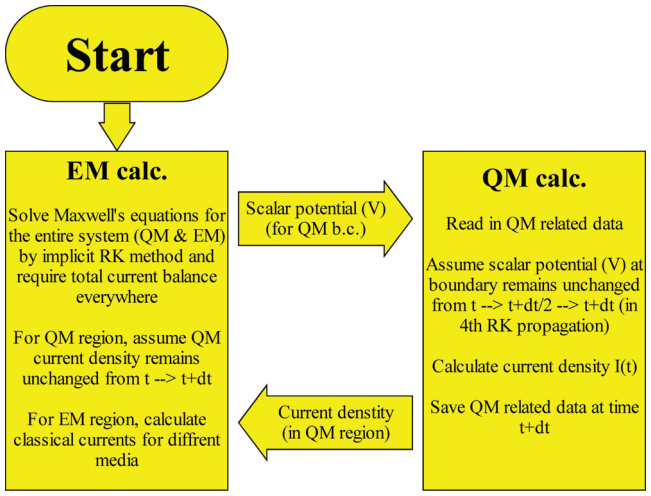

Figure 3. The time-domain QM/EM scheme. Alternate QM and EM calculations at every time step to attain a self-consistent solution of the QM/EM method.

principles. In fact, the calculated dynamic admittance of the QM region is indeed complex.

EXAMPLES AND RESULTS

The time-domain QM/EM method has been applied to a carbon nanotube electronic device connected to two aluminum electrodes with a silicon substrate, and the entire structure has a dimension of $8 \times 5 \times 5$ nm^3. The device, (5, 5) nanotube, and part of the electrodes (in total 128 aluminum atoms and 60 carbon atoms) are enclosed in the QM region with a size of $4 \times 1 \times 1$ nm^3.

Figure 4 shows a cross-sectional view of the three-dimensional device and some characteristic sizes. The conductivity of

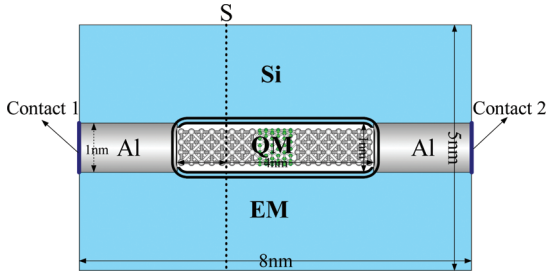

Figure 4. Schematic diagram to illustrate the dynamic multiscale time-domain QM/EM approach. The region enclosed in the central box is simulated by the quantum mechanical transport model with full atomistic details, while the outer EM region is simulated using the coupled EM semiconductor method.

metal electrodes σ is 3.37×10^7 S/m, and an undoped silicon substrate with a relative permittivity of 11.9 is used. FVM discretization generates $15 \times 11 \times 11$ nodes and 4994 links in total. The minimum mesh size, Δl_{min}, is 0.25 nm in the computational grid. According to the Courant stability condition, the maximum time step for explicit methods has to be less than 0.5×10^{-3} fs ($\Delta t_{Cou-Max} = \Delta l_{min}/(c\sqrt{3}) = 0.481 \times 10^{-3}$fs), which is obviously inefficient for the time-domain simulation. By applying the implicit methods, the simulations are stable and relatively accurate, even with a step size several times larger than the Courant stability restraint. The IRK2 method and a time step of 0.02 fs are thus used in all simulations.

The initial state of the time-domain QM/EM simulations is obtained by first grounding both contacts 1 and 2. The static solution is obtained by solving the EM model, which provides the initial condition for the EM part while the initial state of the QM part is obtained by a ground state DFTB simulation. Time-dependent AC signals can then be introduced by applying different boundary voltages on the electrodes. In this work, three typical time-dependent boundary conditions are chosen to test our time-domain QM/EM solver.

In the following simulations, different currents across the surface S in Figure 4 are evaluated to assess the modeling results. These currents include the total current (I_T), the displacement current (I_D), and the conduction current (I_{QM}) from the QM region (calculated by TDDFTB method). The conduction currents around the QM region besides the two ends are very small since the surrounding substrate is the undoped silicon block. Therefore, those currents across S in Figure 4 should approximately satisfy the relationship of $I_T = I_D + I_{QM}$ as verified in following simulations.

1. Case One: Exponential Increasing Bias Voltage.

$$V(\text{contact 1}) = V_{dc} + V_{ac}(1 - e^{-t/a}) \quad \text{(boundary condition)} \tag{63}$$

where $V_{dc} = 0.0$ V and $V_{ac} = 1$ mV.

First, an exponential increasing bias voltage with time constant $a = 1$ fs is applied which corresponds to the rapid switch-on limit. Different currents across the interface S (in Figure 4) are plotted in Figure 5a. These currents reach their steady states

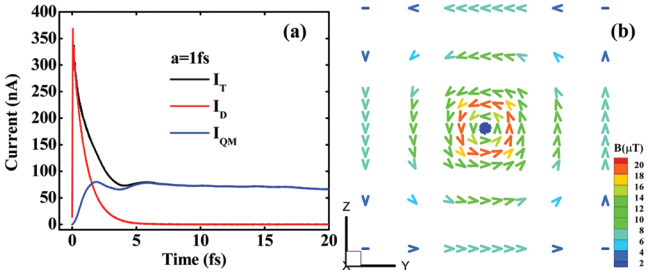

Figure 5. (a) The time-dependent currents across the interface S in Figure 4 under the boundary condition case one with the time constant $a = 1$ fs. The black line, red line, and blue line correspond to the total current I_T, displacement current I_D, and conduction current from the QM region I_{QM}, respectively. (b) The static magnetic field distribution for the steady state with a bias of 1 mV at $t = 20$ fs.

in ~10 fs, and the displacement current I_D gradually diminishes afterward. With the vanishing I_D, the total current I_T is mainly contributed by the conduction current I_{QM}. The static resistance of the system is around 14 kΩ, and the magnetic field distribution is shown as Figure 5b at the steady state with a bias voltage of 1 mV.

However, at the beginning stage (<5 fs), the displacement current is the main component of the total current as shown in Figure 5a, due to the sudden introduction of an electromagnetic field into the system. Therefore, the displacement current should be reduced at the beginning stage when the bias voltage is turned on slowly, as shown in Figure 6. The time-dependent current

dx.doi.org/10.1021/ct200859h | J. Chem. Theory Comput. 2012, 8, 1190–1199

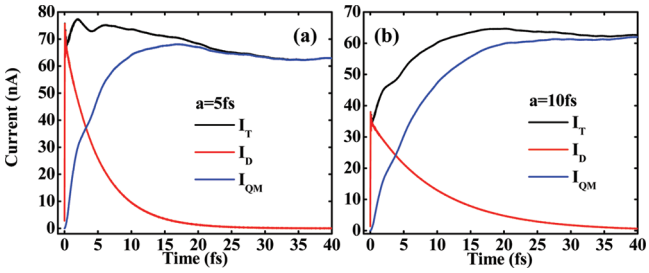

Figure 6. The time-dependent currents across the interface S in Figure 4 under the boundary condition case one: (a) with the time constant a = 5 fs and (b) with the time constant a = 10 fs.

asymptotically approaches the steady state as the time evolves, and full electric and magnetic field distributions for the steady state are shown in Figure 5b.

2. Case Two: Sinusoidal Bias Voltage.

$$V(\text{contact 1}) = V_{dc} + \frac{V_{ac}}{2}\left(1 - \cos\left(\frac{2\pi t}{a}\right)\right)$$

$$(\text{boundary condition}) \qquad (64)$$

where V_{dc} = 0.0 V, V_{ac} = 0.1 mV, and a = 5 fs.

This case corresponds to an excited signal with the frequency f = 200 THz, and the response of the coupled system is displayed in Figure 7. Different phase delays relative to bias voltage,

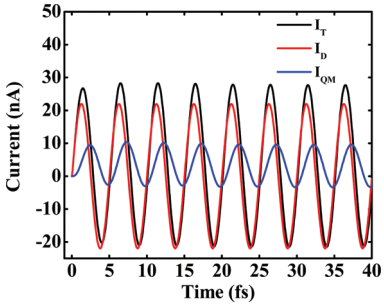

Figure 7. The time-dependent currents across the interface S in Figure 4 under the boundary condition case two (the bias voltage is sinusoidal with a period of 5 fs).

respectively for the total current I_T, displacement current I_D, and conduction current I_{QM}, can be observed as shown in Figure 7. At high operational frequency, the displacement current contributes a significant component to the total current I_T. Therefore, it is necessary to comprehensively consider the electrodynamics effect in the performance assessment of nanodevices.

3. Case Three: Pulsed Bias Voltage.

$$V(\text{contact 1}) = V_{dc} + V_{ac}\exp\left(-\frac{(t - t_c)^2}{a^2}\right)$$

$$(\text{boundary condition}) \qquad (65)$$

where V_{dc} = 0.0 V, V_{ac} = 1 mV, t_c = 20 fs, and a = 5 fs.

The resultant time-dependent currents are displayed in Figure 8; this simulation shows that our TD-QM/EM solver is approximately time-reversal. Furthermore, one could observe an apparent shift for the total current relative to the conduction current by calculating the displacement current in Figure 8.

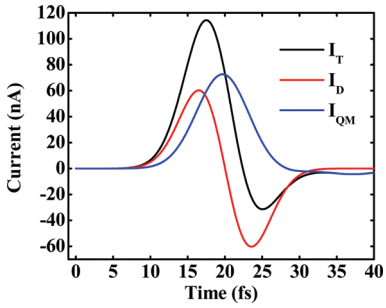

Figure 8. The time-dependent currents across the interface S in Figure 4 under the boundary condition case three.

CONCLUSION

A time-domain multiscale QM/EM method is developed and applied to study the dynamic electrical response of a carbon nanotube based molecular device. The drift-diffusion equation and NEGF formalism for quantum transport coupled with the Maxwell's equations are solved to investigate the interaction between charge particles and electromagnetic field at different temporal and spatial scales. The two charge transport models, the classical and quantum mechanical, are coupled at the interface via the boundary conditions. By solving for the scalar and vector potentials, the time-domain QM/EM method is formulated within a unified framework, and the multiscale dynamics are solved within a seamlessly integrated framework. The time-domain QM/EM method presented in this manuscript is a direct extension of the recently developed QM/EM method for the static field. The TDDFT-NEGF-EOM method is used for the QM simulation with the AWBL approximation. Recently, an improved TDDFT-NEGF-EOM method[23] was proposed to go beyond the AWBL approximation and may be used for the QM part of the simulation. The finite difference method is employed for the EM calculation. Other EM methods can be used as well, for instance, the finite element method. To improve the efficiency further, we may employ the algorithms for sparse matrix manipulation and parallelize the codes. With all of these improvements, we expect that the time-domain QM/EM method can be used routinely to simulate the dynamic response of nanoscopic electronic and optoelectronic devices.

AUTHOR INFORMATION

Corresponding Author

*E-mail: yamcy@yangtze.hku.hk (C.Y.Y.); ghc@everest.hku.hk (G.H.C.).

Notes

The authors declare no competing financial interest.

ACKNOWLEDGMENTS

We acknowledge the financial support from the Hong Kong University Grant Council (AoE/P-04/08), Hong Kong Research Grant Council (HKU700909P, HKUST9/CRF/08, HKU700808P, HKU701307P and HKU718711E), and The University of Hong Kong (UDF on Fast Algorithm, Seed Funding Programme for Basic Research 2010-11159085 and 201010159001, Small Project Funding 201007176060).

REFERENCES

(1) Yam, C.; Meng, L.; Chen, G.; Chen, Q.; Wong, N. *Phys. Chem. Chem. Phys.* **2011**, *13*, 14365.

(2) Yam, C.; Mo, Y.; Wang, F.; Li, X.; Chen, G.; Zheng, X.; Matsuda, Y.; Tahir-Kheli, J.; Goddard-III, W. A. *Nanotechnology* **2008**, *19*, 495203.
(3) Wen, S.; Koo, S.; Yam, C.; Zheng, Xiao; Yan, Y.; Su, Z.; Fan, K.; Cao, L.; Wang, W.; Chen, G. *J. Phys. Chem. B* **2011**, *115*, 5519.
(4) Auf-der-Maur, M.; Povolotskyi, M.; Sacconi, F.; Pecchia, A.; Di-Carlo, A. *J. Comput. Electron.* **2008**, *7*, 398.
(5) Bredas, J.-L.; Norton, J. E.; Cornil, J.; Coropceanu, V. *Acc. Chem. Res.* **2009**, *42*, 1691.
(6) Li, J.; Chan, C. T. *Phys. Rev. B* **2005**, *72*, 195103.
(7) Zhou, L.; Wen, W.; Chan, C. T.; Sheng, P. *Phys. Rev. Lett.* **2005**, *94*, 243905.
(8) Vasileska, D.; Goodnick, S. M. *Computational Electronics*; Morgan & Claypool: San Francisco, CA, 2006.
(9) Meng, L.; Shang, Y.; Li, Q.; Li, Y.; Zhan, X.; Shuai, Z.; Kimber, R. G. E.; Walker, A. B. *J. Phys. Chem. B* **2010**, *114*, 36.
(10) Meng, L.; Wang, D.; Li, Q.; Yi, Y.; Bredas, J.-L.; Shuai, Z. *J. Chem. Phys.* **2011**, *134*, 124102.
(11) Shang, Y.; Li, Q.; Meng, L.; Wang, D.; Shuai, Z. *Appl. Phys. Lett.* **2010**, *97*, 143511.
(12) Runge, E.; Gross, E. K. U. *Phys. Rev. Lett.* **1984**, *52*, 997.
(13) Yam, C.; Yokojima, S.; Chen, G. *Phys. Rev. B* **2003**, *68*, 153105.
(14) Yam, C.; Yokojima, S.; Chen, G. *J. Chem. Phys.* **2003**, *119*, 8794.
(15) Yam, C.; Zheng, X.; Chen, G.; Wang, Y.; Frauenheim, T.; Niehaus, T. A. *Phys. Rev. B* **2011**, *83*, 245448.
(16) Zheng, X.; Wang, F.; Yam, C. Y.; Mo, Y.; Chen, G. *Phys. Rev. B* **2007**, *75*, 195127.
(17) Ke, S.-H.; Liu, R.; Yang, W.; Baranger, H. U. *J. Chem. Phys.* **2010**, *132*, 234105.
(18) Stefanucci, G.; Almbladh, C.-O. *Phys. Rev. B* **2004**, *69*, 195318.
(19) Kurth, S.; Stefanucci, G.; Almbladh, C.-O.; Rubio, A.; Gross, E. K. U. *Phys. Rev. B* **2005**, *72*, 035308.
(20) Yuen-Zhou, J.; Tempel, D. G.; Rodríguez-Rosario, C. A.; Aspuru-Guzik, A. *Phys. Rev. Lett.* **2010**, *104*, 043001.
(21) Wang, B.; Xing, Y.; Zhang, L.; Wang, J. *Phys. Rev. B* **2010**, *81*, 121103.
(22) Di-Ventra, M.; D'Agosta, R. *Phys. Rev. Lett.* **2007**, *98*, 226403.
(23) Zheng, X.; Chen, G.; Mo, Y.; Koo, S.; Tian, H.; Yam, C.; Yan, Y. *J. Chem. Phys.* **2010**, *133*, 114101.
(24) Kadanoff, L. P.; Baym, G. *Quantum statistical mechanics: Green's function methods in equilibrium and nonequilibrium problems*; Addison-Wesley: Reading, MA, 1989.
(25) Griggiths, D. J. *Introduction to electrodynamics*; Prentice-Hall: New York, 1999.
(26) Chew, W. C.; Tong, M. S.; Hu, B. *Integral Equation Methods for Electromagnetic and Elastic Waves*; Morgan & Claypool: San Francisco, CA, 2009.
(27) Ayubi-Moak, J. S.; Goodnick, S. M.; Aboud, S. J.; Saraniti, M.; El-Ghazaly, S. *J. Comput. Electron.* **2003**, *2*, 183.
(28) Ayubi-Moak, J. S.; Goodnick, S. M.; Saraniti, M. *J. Comput. Electron.* **2006**, *5*, 415.
(29) Willis, K. J.; Ayubi-Moak, J. S.; Hagness, S. C.; Knezevic, I. *J. Comput. Electron.* **2009**, *8*, 153.
(30) Willis, K. J.; Hagness, S. C.; Knezevic, I. *Appl. Phys. Lett.* **2010**, *96*, 062106.
(31) Grondin, R. O.; El-Ghazaly, S. M.; Goodnick, S. *IEEE Trans. Microwave Theory Tech.* **1999**, *47*, 817.
(32) Meuris, P.; Schoenmaker, W.; Magnus, W. *IEEE Trans. Comput.-Aided Des.* **2001**, *20*, 753.
(33) Schoenmaker, W.; Meuris, P. *IEEE Trans. Comput.-Aided Des.* **2002**, *21*, 534.
(34) Eymard, R.; Gallouet, T.; Herbin, R. *Finite Vol. Methods, ser. Handbook of Numerical Analysis*; Elsevier: Amsterdam, 2000; Vol. 7.
(35) Magwel. http://www.magwel.com/ (accessed March 2012).
(36) Hoefer, W. J. R. *IEEE Trans. Microwave Theory Tech.* **1992**, *40*, 1517.
(37) Zheng, F.; Chen, Z.; Zhang, J. *IEEE Microwave Guided Wave Lett.* **1999**, *9*, 441.
(38) Taflove, A.; Hagness, S. C. *Computational Electrodynamics: The Finite-Difference Time-Domain Method*, 3rd ed.; Artech House: London, 2005.
(39) Alexander, R. *SIAM J. Numer. Anal.* **1977**, *14*, 1006.
(40) Spiteri, R. J.; Dean, R. C. *IEEE Trans. Biomed. Eng.* **2008**, *55*, 1488.
(41) Scharfetter, D. L.; Gummel, H. K. *IEEE Trans. Electron Devices* **1969**, *16*, 64.
(42) Courant, R.; Friedrichs, K.; Lewy, H. *IBM J. Res. Dev.* **1967**, *11*, 215.
(43) Willis, K. J.; Hagness, S. C.; Knezevic, I. *J. Appl. Phys.* **2011**, *110*, 063714.
(44) Porezag, D.; Frauenheim, T.; Köhler, T.; Seifert, G.; Kaschner, R. *Phys. Rev. B* **1995**, *51*, 12947.
(45) Elstner, M.; Porezag, D.; Jungnickel, G.; Elsner, J.; Haugk, M.; Frauenheim, T.; Suhai, S.; Seifert, G. *Phys. Rev. B* **1998**, *58*, 7260.
(46) Keldysh, L. V. *Sov. Phys. JETP* **1965**, *20*, 1018.
(47) Wang, Y.; Yam, C.-Y.; Frauenheima, T.; Chen, G. H.; Niehaus, T. A. *Chem. Phys.* **2011**, *391*, 69.
(48) Ghosh, S. K.; Dhara, A. K. *Phys. Rev. A* **1988**, *38*, 1149.